

Structured scintillator for hard x-ray grating interferometry

Simon Rutishauser,^{1,a)} Irene Zanette,² Tilman Donath,¹ Anna Sahlholm,³
Jan Linnros,⁴ and Christian David¹

¹Paul Scherrer Institut, CH-5232 Villigen PSI, Switzerland

²European Synchrotron Radiation Facility, F-38043 Grenoble, France

³Scint-X AB, 16440 Kista-Stockholm, Sweden

⁴Royal Institute of Technology, 16440 Kista-Stockholm, Sweden

(Received 14 January 2011; accepted 7 April 2011; published online 27 April 2011)

Grating interferometry at conventional x-ray tubes improves the quality of radiographies and tomograms by providing phase and scattering contrast data. The main challenge encountered when applying this technique at high photon energies, as required by many applications to obtain sufficient penetration depth, is to maintain a high fringe visibility. In this letter, we report on a substantial improvement in fringe visibility and according improvements in image quality achieved by replacing the absorbing analyzer grating of the interferometer with a structured scintillator grating. This development represents a significant step toward the implementation of this technique in industrial testing and medical applications. © 2011 American Institute of Physics.

[doi:10.1063/1.3583464]

Conventional x-ray imaging and tomography rely on attenuation as contrast mechanism. Albeit this provides good contrast for many applications, where strongly absorbing objects are imaged, phase contrast imaging can potentially provide much higher contrast, especially in soft tissue and other low-absorbing materials.^{1,2}

Differential phase contrast imaging using a grating interferometer has been developed over the last few years, first at highly brilliant synchrotron sources with monochromatic and almost parallel beam.³⁻⁵ Introducing an additional absorbing source grating to the setup, it was implemented at conventional low-brilliance x-ray tubes,^{6,7} opening the path to widespread application in commercial x-ray imaging tools. The improved image quality of grating based x-ray phase contrast on an x-ray tube was recently demonstrated on a medical sample.⁸ In addition to the quantitative attenuation and differential phase information, grating interferometry also yields a dark field signal, related to small-angle scattering from structures smaller than the spatial resolution of the detector, for instance the fine inner structures of bones.⁹

The experiments cited above were performed at photon energies up to 28 keV. Most clinical, industrial testing and security applications, however, require the use of higher x-ray energies. Recently, an interferometer with a mean photon energy of 60 keV has been implemented at a conventional x-ray tube.¹⁰ The main challenge in this energy range lies in the fabrication of absorption gratings with sufficiently high-absorbing gold structures to provide good image contrast. Transmission of the absorbing grating lines causes a decrease in fringe visibility which deteriorates the image quality.⁵ A potential replacement for the source grating, circumventing this limitation, is the use of a multiline x-ray source.¹¹ In this letter, we report on a structured scintillator, replacing the analyzer grating.

The layout of the grating interferometer is shown in Fig. 1. It consists of a phase grating G_1 of period p_1 with π phase shifting lines, which creates a line interference pattern. The

source grating G_0 is introduced to ensure sufficient spatial coherence. It divides the source into many mutually incoherent line sources, each of which adds constructively (but incoherently) to the interference pattern.⁷ The period of the interference pattern is in the order of microns and typically much smaller than the detector spatial resolution. In order to determine its lateral position and amplitude, which are related to the differential phase and scattering properties of the sample, an analyzer grating G_2 is used. It is scanned over one or several periods, perpendicular to both optical axis and grating lines. This phase stepping scan yields an oscillating signal at each pixel [Fig. 2(a)], whose visibility V is of pivotal importance to the quality of both the differential phase and the dark field signal.

The oscillating signal from the phase stepping scan can be written as a Fourier series for each pixel⁹

$$I(m, n, x_g) = \sum_k a_k(m, n) \cos \left[k \frac{2\pi}{p_2} x_g + \varphi_k(m, n) \right], \quad (1)$$

where (m, n) are the pixel coordinates, x_g is the normalized phase stepping position, a_k are the amplitude coefficients, and φ_k the phase of the Fourier components. The normalized transmission at each pixel is given by $T(m, n) = a_0/a_0^r$, where the superscript r designates values extracted from a reference

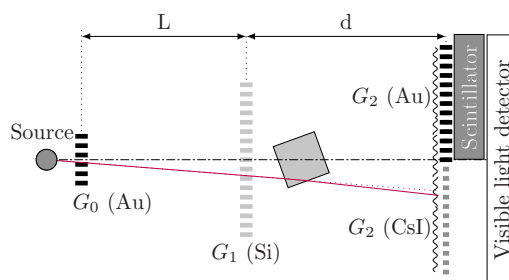


FIG. 1. (Color online) Grating interferometer with absorbing source grating G_0 , phase shifting grating G_1 and analyzer grating G_2 . The conventional absorbing analyzer grating and its separate, continuous scintillator (top half) are replaced by the structured scintillator grating, presented in this letter (bottom half).

^{a)}Electronic mail: simon.rutishauser@psi.ch.

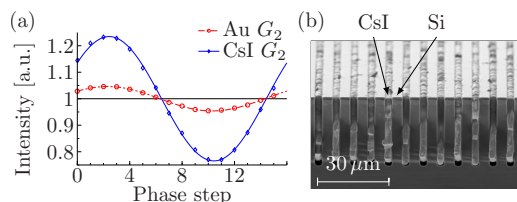


FIG. 2. (Color online) (a) Intensity of a pixel in a phase stepping scan over one grating period in 16 steps for both setups. (b) Scanning electron micrograph of the CsI filled analyzer grating.

scan recorded without object in the beam. For a phase stepping scan over k periods, the difference in fringe phase $\Delta\varphi = \varphi_k - \varphi_k^r$ is proportional to the refraction or diffraction angle from the object. This is illustrated by the solid (refracted by the object) and dotted (nonrefracted reference) rays traced in Fig. 1. The fringe shift is also proportional to the differential phase of the wavefront.⁵ The normalized fringe visibility $\hat{V}(m, n) = (a_k/a_0)/(a_k^r/a_0^r)$ yields a dark field signal.⁹

The root mean square (rms) noise on the transmission signal only has a one over square-root dependence on the number of photons N . For the differential phase contrast signal, however, the rms noise is also inversely proportional to the fringe visibility $V(m, n) = a_k/a_0$ as shown in Ref. 12 [Eq. (25)]

$$\sigma_\varphi \propto \frac{1}{V\sqrt{N}}. \quad (2)$$

An equivalent relation also holds for the noise of the dark field signal $\sigma_{\hat{V}}$. These relations demonstrate, that visibility has a much stronger, proportional impact on the signal quality, and is hence of greater importance than the number of photons.

To compare the performance of a grating interferometer with a structured scintillator to a conventional configuration, a symmetric interferometer with grating periods $p_{0,1,2} = 8.5 \mu\text{m}$ and intergrating distances $L=d=875 \text{ mm}$ was implemented (Fig. 1).¹⁰ The source grating G_0 was made of two stacked gratings, each with $90 \mu\text{m}$ high gold lines. The π shifting phase grating G_1 was made of silicon structures with a height of $h_1=75 \mu\text{m}$. The gratings were manufactured in a process involving photolithography, deep etching into silicon and electroplating of gold.¹³

In the conventional setup, the absorption grating G_2 was made of $90 \mu\text{m}$ high gold structures. Downstream of G_2 , the x-rays are converted to visible light by a columnar growth cesium iodide (CsI) scintillator of $150 \mu\text{m}$ thickness (Hamamatsu).

In the structured scintillator setup, the combination of absorption grating G_2 and scintillator was replaced by a structured scintillator grating of same pitch as the absorption G_2 , a structure height of $h_2=30 \mu\text{m}$ and an area of $30 \times 30 \text{ mm}^2$ [Fig. 2(b)]. The scintillator grating was made of silicon which had been surface oxidized and filled with thallium doped CsI.¹⁴

The x-ray tube with a tungsten target was operated at 90 kV and a source point diameter of 1 mm (Comet MXR-160HP/11). With 17 mm aluminum prefiltering, the spectrum had a mean energy of 59 keV, which coincides with the tungsten $K\alpha_1$ emission line. The images were recorded by a lens coupled Peltier cooled charge coupled device (Fingerlake In-

struments Proline) with 1024×1024 pixels and an effective pixel size of $93 \mu\text{m}$, using 2×2 pixel binning.

Experiments using the reference setup with absorption analyzer grating show an average fringe visibility of $V = a_k^r/a_0^r = 5.3\%$. The structured scintillator setup shows a strongly improved visibility of $V=22.2\%$. These values correspond to the amplitude of the normalized phase stepping signals in Fig. 2(a). The observed visibility improvement by a factor of 4.2 even slightly exceeds the factor of 3.5 that can be expected from wave-optical simulations. The increased visibility results in an improved signal quality for both the differential phase contrast and the dark field signal.

As test object we used a square shaped aluminum profile. It was mounted as indicated in Fig. 1, rotated by $\approx 20^\circ$ with respect to the imaging plane to give three regions with positive, zero and negative phase gradient, respectively [Fig. 3(a)]. Its differential phase contrast signal is shown in Figs. 3(a)–3(d). Based on Eq. (2) and the measured visibilities in reference scans, the rms noise observed using the absorption grating is expected to be about 4.2 times higher than with the structured scintillator. This is confirmed by the factor of 5.4 observed in the experiment at 5500 detector counts [Figs. 3(b) and 3(d)]. Even by increasing the number of detector counts to 50 000 as shown in Fig. 3(c), the image obtained with the conventional setup does not achieve the quality of the image obtained with the structured scintillator. Both the expected and measured rms noise improvement amount only to a factor of 3.

A second example illustrates the improvements in dark field signal quality due to the structured scintillator. Figures 3(e)–3(h) show the dark field signal $\hat{V}(m, n)$ obtained from different paper layer thicknesses. At the same detector count, the standard deviation of measured \hat{V} within a region of constant scattering is 4.5 times lower with the structured scintillator. As with the differential phase signal, the noise level in the conventional setup can be reduced by increasing the exposure times, without achieving the signal quality obtained with the structured scintillator [Fig. 3(g)].

In the current implementation, the improvement in signal quality comes at the cost of increased exposure times. A detector count of 5500 requires a 60 s exposure using the structured scintillator, which is a factor of 70 longer than with the absorption grating setup (Fig. 3). This efficiency difference can be attributed to a combination of several factors: different thickness in the scintillator material, unwanted transmission through the absorbing G_2 grating and the difficulty of coupling the isotropically emitted light out of the high aspect ratio microstructures of the structured scintillator. In order to improve the efficiency of the device, modifications of the light guiding properties such as coating the grating structures with a layer of reflecting material in combination with an increased structure height can be envisaged. Other potentially contributing factors are incomplete, inhomogeneous filling of the trenches and a partial loss of thallium doping in the fabrication process.¹⁴

In summary we have demonstrated the implementation of a structured scintillator as analyzer grating for grating interferometry. It shows a substantial increase in fringe visibility at x-ray energies around 60 keV, leading to a strong improvement in the quality of the recorded differential phase and dark field data compared to a conventional grating interferometry setup with absorption grating. The considerably

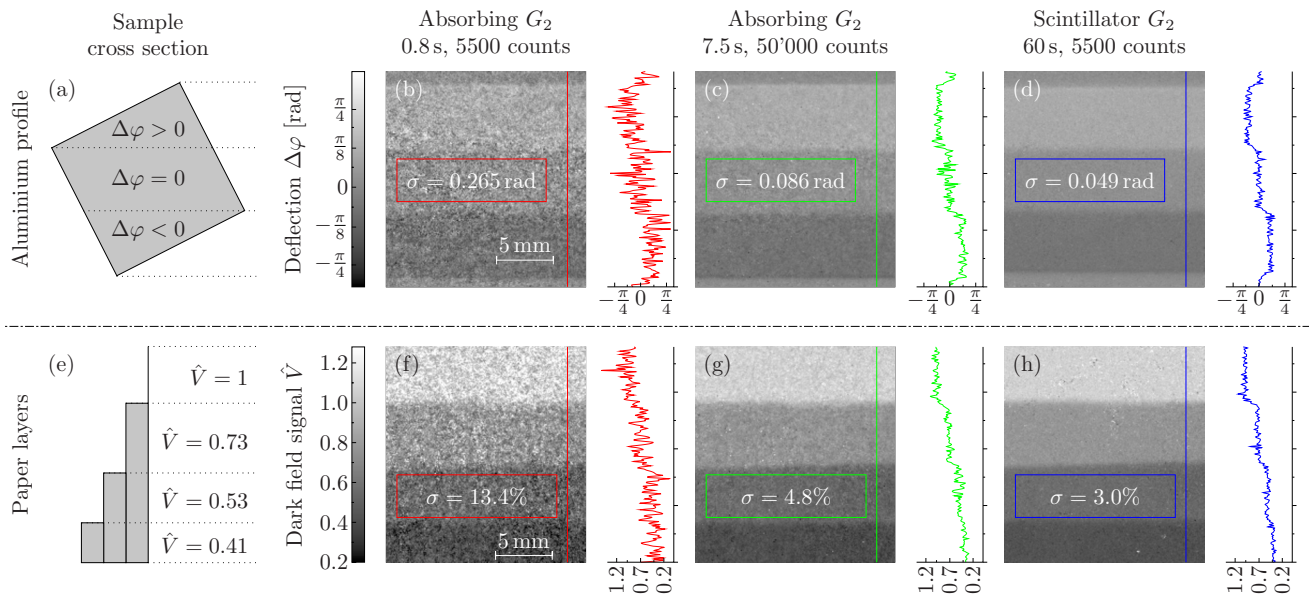


FIG. 3. (Color online) Differential phase contrast images of a square aluminum profile [(a)–(d)] and dark field images of zero (at the top), one, two, and three layers of paper [(e)–(h)]. The cross sections of both samples are sketched [(a) and (e)]. They are imaged using the absorption analyzer grating at 5500 counts [(b) and (f)], the absorption analyzer grating at 50 000 counts [(c) and (g)], and the structured scintillator at 5500 detector counts [(d) and (h)]. The exposure times are specified in seconds per phase step. Next to each image is a profile along the plotted vertical lines. The standard deviation σ (rms noise) is given within the marked rectangular regions of constant differential phase or scattering power respectively.

lower conversion efficiency of this first implementation is supposed to stem from nonoptimal scintillator grating properties, leaving room for improvement. Already in its current state, the device is of great interest for use at synchrotron sources, where due to the much higher flux, conversion efficiency is less of a concern and thin scintillators are commonly used for high resolution applications.

The authors would like to thank Martin Bednarzik for grating fabrication, Venera Altapova for assisting at the first experiments, Oliver Bunk for his help in computing and hardware interfacing and Olof Svenonius for discussions on scintillator efficiency.

¹R. Fitzgerald, *Phys. Today* **53**(7), 23 (2000).

²A. Momose, *Jpn. J. Appl. Phys., Part 1* **44**, 6355 (2005).

³C. David, B. Nöhammer, H. Solak, and E. Ziegler, *Appl. Phys. Lett.* **81**, 3287 (2002).

⁴A. Momose, *Opt. Express* **11**, 2303 (2003).

⁵T. Weitkamp, A. Diaz, C. David, F. Pfeiffer, M. Stampanoni, P. Cloetens, and E. Ziegler, *Opt. Express* **13**, 6296 (2005).

⁶F. Pfeiffer, T. Weitkamp, O. Bunk, and C. David, *Nat. Phys.* **2**, 258 (2006).

⁷T. Weitkamp, C. David, C. Kottler, O. Bunk, and F. Pfeiffer, *Proc. SPIE* **6318**, 63180S (2006).

⁸T. Donath, F. Pfeiffer, O. Bunk, C. Grünzweig, E. Hempel, S. Popescu, P. Vock, and C. David, *Invest. Radiol.* **45**, 445 (2010).

⁹F. Pfeiffer, M. Bech, O. Bunk, P. Kraft, E. F. Eikenberry, C. Brönnimann, C. Grünzweig, and C. David, *Nature Mater.* **7**, 134 (2008).

¹⁰T. Donath, F. Pfeiffer, O. Bunk, W. Groot, M. Bednarzik, C. Grünzweig, E. Hempel, S. Popescu, M. Hoheisel, and C. David, *Rev. Sci. Instrum.* **80**, 053701 (2009).

¹¹A. Momose, W. Yashiro, H. Huwahara, and K. Kawabata, *Jpn. J. Appl. Phys.* **48**, 076512 (2009).

¹²K. Engel, D. Geller, T. Köhler, G. Martens, S. Schusser, G. Vogtmeier, and E. Rössl, *Nucl. Instrum. Methods Phys. Res. A* (to be published).

¹³C. David, J. Bruder, T. Rohbeck, C. Grünzweig, C. Kottler, A. Diaz, O. Bunk, and F. Pfeiffer, *Microelectron. Eng.* **84**, 1172 (2007).

¹⁴P. Kleimann, J. Linnros, C. Fröjd, and C. Petersson, *Nucl. Instrum. Methods Phys. Res. A* **460**, 15 (2001).